Korean Journal of Remote Sensing, Vol.24, No.1, 2008, pp.1~16

A Remote Sensed Data Combined Method for Sea Fog Detection

Ki-Young Heo*, Jae-Hwan Kim*, Jae-Seol Shim, Kyung-Ja Ha*†, Ae-Sook Suh***, Hyun-Mi Oh*, and Se-Yun Min***

*Division of Earth Environmental System, College of Natural Science, Pusan National University, Busan, 609-735, Republic of Korea

**Coastal Disaster Prevention Research Division, Korea Ocean Research & Development Institute, Ansan, 426-744, Republic of Korea

***Environmental and Meteorological Satellite Division, Korean Meteorological Administration, Seoul, 156-720, Republic of Korea

Abstract : Steam and advection fogs are frequently observed in the Yellow Sea from March to July except for May. This study uses remote sensing (RS) data for the monitoring of sea fog. Meteorological data obtained from the Ieodo Ocean Research Station provided a valuable information for the occurrence of steam and advection fogs as a ground truth. The RS data used in this study were GOES-9, MTSAT-1R images and QuikSCAT wind data. A dual channel difference (DCD) approach using IR and shortwave IR channel of GOES-9 and MTSAT-1R satellites was applied to detect sea fog.

The results showed that DCD, texture-related measurement and the weak wind condition are required to separate the sea fog from the low cloud. The QuikSCAT wind data was used to provide the wind speed criteria for a fog event. The laplacian computation was designed for a measurement of the homogeneity. A new combined method, which includes DCD, QuikSCAT wind speed and laplacian computation, was applied to the twelve cases with GOES-9 and MTSAT-1R. The threshold values for DCD, QuikSCAT wind speed and laplacian are -2.0 K, 8 m s^{-1} and 0.1, respectively. The validation results showed that the new combined method slightly improves the detection of sea fog compared to DCD method: improvements of the new combined method are 5 ~ 6 % increases in the Heidke skill score, 10% decreases in the probability of false detection, and 30 ~ 40% increases in the odd ratio.

Key Words : Sea fog; Low cloud; Remote sensing; Laplacian; Homogeneity.

1. Introduction

Fog is defined as a phenomenon with a horizontal visibility of less than 1 km near the surface over both ocean and land (Byers, 1959; Roach, 1994). The monitoring and forecasting of fog is an imperative task, because fog is responsible for automobile accidents, aircraft takeoff and landing problems, and

Received 5 November 2007; Accepted 8 January 2008.

† Corresponding Author: Kyung-Ja Ha (kjha@pusan.ac.kr)

marine accidents due to poor visibility. Generally, fog consists of micro-scale and meso-scale rather than a synoptic scale in space and time, with characteristic scales of hours in time and of tens km in horizontal scale. Therefore, the formation and dissipation of fog and low level stratus is difficult to predict using numerical weather forecast models (Croft *et al.*, 1997). In weather forecasting only the potential possibility or pre-condition for fog can be predicted, mainly from empirical relationships.

In Korea it has been reported that the occurrence of sea fog in the southwestern sea or the Yellow Sea is maximum in July, mainly due to air-sea temperature differences, as the result of warm air advection and formation of cold water pool (Cho *et al.*, 2000; Fu *et al.*, 2006). This advection-type fog is generally considered to be a typical sea fog in the middle latitudes under stable conditions over the cold sea surface temperature (Klein and Hartmann, 1993). The observation stations located at the coastal zone and the IORS (Ieodo Ocean Research Station) can provide the ground truth. The IORS data has been especially useful in formulating the synopsis for fog formation in the Yellow Sea with sea surface temperature, wind, air temperature, and humidity as well as visibility. The time evolution of fog event was informed by the IORS data.

Methods using station observations, however, are limited, due to the lack of an observation network. Remote sensing (RS) monitoring via satellite observation is required to locate the area covered by fog. Eyre *et al.* (1984) and Park *et al.* (1997) introduced a method using dual-channel radiometers with two infrared channels, shortwave IR (3.7μm) and longwave IR (11μm) of the National Oceanic and Atmospheric Administration (NOAA) Advanced Very High Resolution Radiometer (AVHRR) to detect nocturnal fog and low stratus. However, it was limited to monitoring the temporal variation of a fog event at 12 hour intervals due to the low earth orbit of the NOAA satellite. Since 2003 GOES-9 (Geostationary Operational Environmental Satellite) data was serviced, this study examines the monitoring method of DCD using 3.9 μm and 10.7 μm of GOES-9 in 2004 for sea fog in the Yellow Sea, which is comprised of snapshots at 30-minute intervals. The application of DCD on GOES-9 will be useful for comparison with the MTSAT-1R results since the MTSAT-1R (the Multi-functional Transport Satellite-1 Replacement) launched on 26 February 2005 is equipped with almost the same channels as those of GOES-9. However, the DCD has a limit to distinguish fog from low clouds.

Recently, there have been several studies on the discrimination between fog and low clouds. Bendix *et al.* (2005) and Cermak and Bendix (2005) provided a proper ground fog detection scheme using the comparison of terrain height and the cloud base height computed from cloud top height and cloud geometrical thickness. Guidard and Tzanos (2005) provided relevant information for the potential of fog detection using the relative humidity of ground observation.

In the present study, a new combined method of DCD, QuikSCAT wind speed and laplacian, is evaluated to detect sea fog. The QuikSCAT surface wind is provided as wind conditions for the fog event, and a laplacian method for splitting of sea fog and low cloud is proposed after applications of DCD and QuikSCAT wind. In addition, similarities and differences of this fog detection method between GOES-9 and MTSAT-1R images are examined.

2. Data and methods

1) Data

The data for this study are composed of the surface

observations and satellite images including GOES-9, MTSAT-1R and QuikSCAT. The observation data were used to identify fog events and to verify the result of fog detection using satellite images during fog seasons (April to July) from 2004 trough 2007. The IORS, which is an installed artificial ocean platform located in the East China Sea, provides the data of visibility, sea surface temperature, air temperature, humidity, wind, and surface fluxes per 10 minutes. The AWS (automatic weather station) stations in the coastal zone and the IORS used for the study are shown in Fig. 1.

We used the satellite images from GOES-9 (for the period April to July 2004) and MTSAT-1R (for the period June 2006 to March 2007) with the SWIR (shortwave infrared, 3.9 μm for GOES-9 and 3.8 μm for MTSAT-1R) and LWIR (longwave infrared, 10.7 μm for GOES-9 and 10.8 μm for MTSAT-1R) channels to monitor the area of the fog with time. The GOES-9 satellite provided snapshot data for GVAR (GOES variable), 44 times per day with five channels. The MTSAT-1R satellite has also five channels which consist of four infrared window channels and one visible window channel. These two satellites are observed by the 4 km IR resolution enough to monitor sea fog.

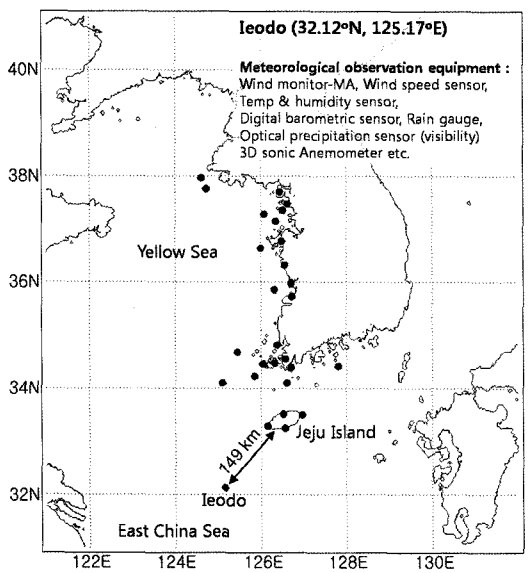

Fig. 1. Geographic map of the Korean Peninsula. AWS stations and the Ieodo Ocean Research Station (IORS) referred in the text are presented.

For the purpose to detect weak wind area, the QuikSCAT data with a spatial resolution of 25 km was used for the period April 2004 to March 2007. The QuikSCAT was launched by the NASA in June 1999 to measure winds near the ocean surface, available twice a day. More detailed information such as the principle of scatterometry and the accuracy of data and historical scientific applications related to QuikSCAT data were previously introduced by Liu *et al.* (1998; 2000; 2001). The validation study (e.g., Wentz *et al.*, 2001) using QuikSCAT and buoy measurements showed that there was very small difference in wind speed with the root-mean-square differences are 0.7 m s^{-1}.

2) Methods

Usually fog occurs during nocturnal time, when the satellite IR channels are available. During the nighttime, the detection of fog using IR images is difficult since the temperature of fog and the underlying surfaces are similar (Scorer, 1986) and there may be a surface inversion (Anthis and Cracknell, 1999). Therefore, a dual-channel method is used to detect foggy areas during the nighttime, as suggested by Eyre *et al.* (1984), Ellrod (1995, 2000). Basically this dual-channel difference (DCD) method uses the difference in emissivity of SWIR and LWIR of GOES-9 for opaque water clouds. At around 11 μm, the brightness temperature (BT) is almost equal to the cloud top temperature (CTT) because opaque water clouds emit radiation as a black body ($\varepsilon \approx 1$). At around 3.7 μm, the BT is significantly lower than CTT due to lower emissivity of 0.8 - 0.9 (Hunt, 1973; Eyre *et al.*, 1984; Park *et al.*, 1997). Therefore, the difference between the BT from the two channels is

sensitive to the presence of fog or low clouds (Anthis and Cracknell, 1999). For example, the different BTs in the case of opaque water cloud are respectively detected -8 °C and 7 °C. This difference is due to different emissivity between two channels as shown in Fig. 2.

To discriminate between fog and low cloud after application of DCD method, we firstly applied the wind speed criteria with QuikSCAT and AWS to application result of DCD method based on the result from Heo and Ha (2004). The result showed that the weak wind speed were necessary conditions for fog formation because the strong winds could dissipate fog or cause it to rise and become stratus. The laplacian operation of BT distribution of channels was secondly developed to separate an area of fog from a large spatial area of negative DCD. It should be noted that the primary responsibility of fog is homogeneous in the horizontal distribution of the BT compared to low cloud (Meteorological Satellite Center, 2002). The laplacian operator of BT, which is represented by $\nabla^2(\mathbf{BT})$, was defined as the divergence of the BT gradient and used as a measure of uniformity. That uses the following equation:

$$\nabla^2(BT) = \frac{\partial^2(BT)}{\partial^2 x} + \frac{\partial^2(BT)}{\partial^2 y} \quad \cdots(1)$$
$$= BT_{i,j-1} + BT_{i,j+1} + BT_{i-1,j} + BT_{i+1,j} - 4 \times BT_{i,j}$$

where $BT_{i,j}$ means brightness temperature at position (i, j) in the x (zonal) and y (meridional) direction. It is known that the BT in a cloudy region is more variable than that in a cloudless region (Coakley and Bretherton, 1982). The laplacian operator is useful for detecting variable BT regions, or, cloudy regions (Sakaida and Kawamura, 1996). In the present study, to remove noise and low cloud in fog detection, the small value of laplacian and weak wind speed condition were verified as proper conditions for sea fog formation.

3. The cases and the DCD method

1) Fog cases

The IORS synoptic observation provides a different time evolution of steam fog and advection fog. For the day examined, the steam fog on 7 April

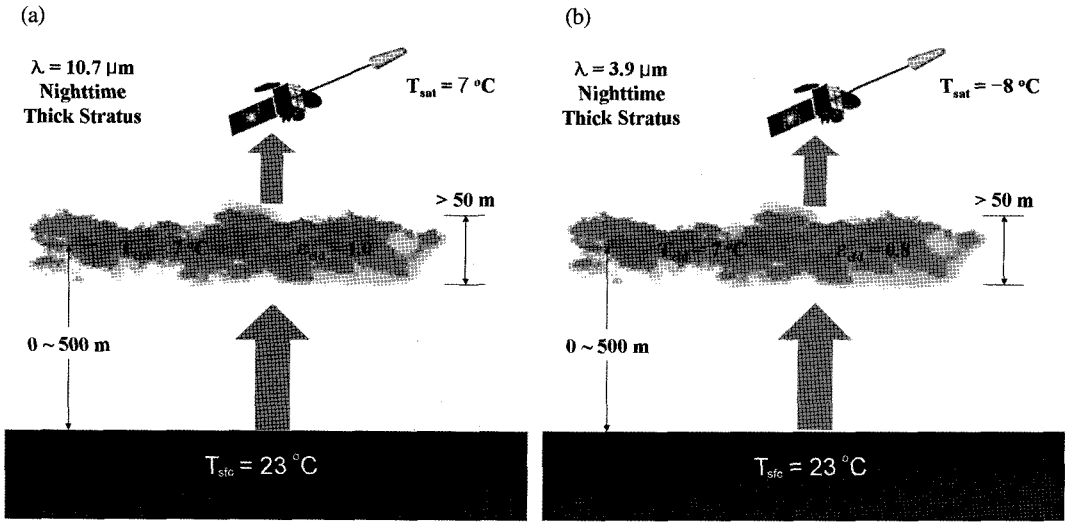

Fig. 2. Emissivity difference of opaque water clouds in the nighttime for channels of (a) 10.7 and (b) 3.9 μm. The different brightness temperatures when the 3.9 μm channel has low emissivity near 0.8 for low cloud and fog with water vapor, the satellite primarily senses energy emitted from cloud top.

2004 appears to be due to the temperature difference between the air and water, which is abrupt and is caused by change in wind direction, wind speed and relative humidity as shown in Fig. 3 (a). This steam fog has a reverse air-sea temperature difference compared with advection fog in Fig. 3 (b). The fog was recorded during the nocturnal period from 04 LST of 400m visibility with a cold air burst over the warmer ocean. The conversion from UTC to LST requires addition of 9 hours (*e.g.*, 09 LST should be understood as 00 UTC). The cold air clearly originated from the northerly wind and both the wind direction and the speed of wind changed at the time of the fog. When the wind speed increases again, the fog is dissipated. In the case of an advection fog, rapid decreases in sea surface temperature were often observed. Before foggy weather with a visibility less than 1 km, the southerly wind was very strong and the air temperature was rapidly increased by 1°C for hours before. At the time of fog formation, the warm air temperature overlies the cold water under the stable conditions with weak wind.

(a) 00 LST 6 to 24 LST 7 April 2004 (steam fog case)

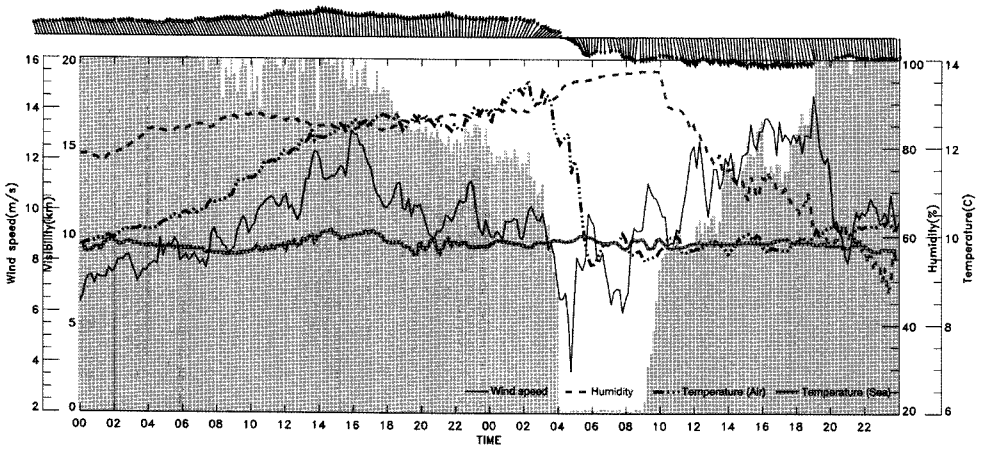

(b) 00 LST 10 to 24 LST 11 June 2005 (advection fog case)

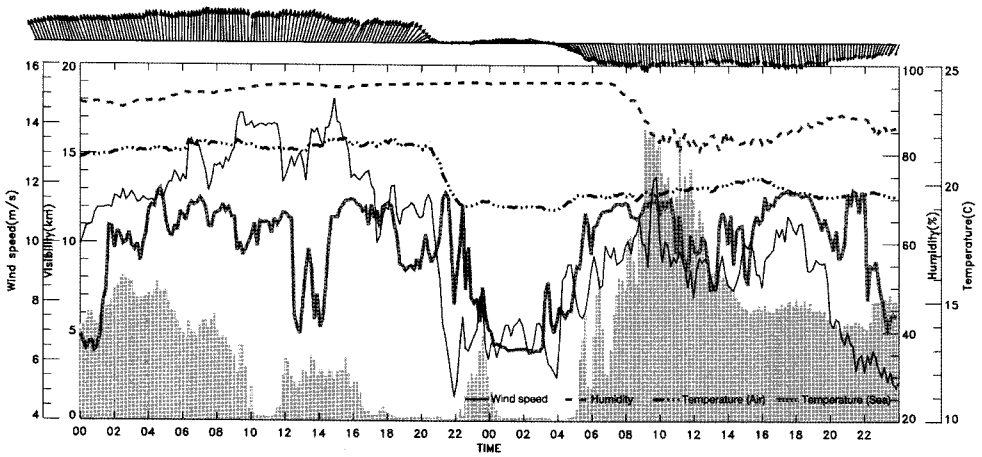

Fig. 3. Time variation of wind speed (solid line), wind direction (wind barb), humidity (dashed line), air temperature (dashed dot line), sea surface temperature (thick solid line) and visibility (shaded area) during the fog events (a) from 00 LST 6 to 24 LST 7 April 2004 and (b) from 00 LST 10 to 24 LST 11 June 2005 at IORS.

Table 1. DCD threshold value using GOES-9 satellite for fog cases at synoptic station

Cases days	Start (LST)	End (LST)	Period	DCD threshold (mean)	Fog type
7 April 2004	0400	0900	5 hours	-2.0	steam fog
9 June 2004	0500	0600	1 hour	-3.8	advection fog
9 ~ 10 June 2004	1830	0530	11 hours	-3.7	advection fog
8 July 2004	0300	0600	4 hours	-2.1	advection fog
8 ~ 9 July 2004	2100	0900	12hours	-2.6	advection fog
10 July 2004	0000	0300	3 hours	-2.2	advection fog
Total time period			36 hours		
Hourly mean of DCD			-2.8		

Table 2. Same as in Table 1 except for MTSAT-1R

Cases days	Start (LST)	End (LST)	Period	DCD threshold (mean)	Fog type
5 June 2006	0000	0600	6 hours	-2.5	advection fog
25 June 2006	0000	0600	6 hours	-2.5	advection fog
26~27 June 2006	2100	0500	8 hours	-3.0	advection fog
28~29 June 2006	2100	0500	8 hours	-3.0	advection fog
2~3 July 2006	2100	0500	8 hours	-2.8	advection fog
27~28 March 2007	2100	0600	9 hours	-2.7	steam fog
Total time period			45 hours		
Hourly mean of DCD			-2.8		

In the present study, to examine the fog detection using GOES-9 and MTSAT-1R images, the twelve cases are evaluated. The twelve fog cases, which include five cases of advection fog and a case of steam fog, are presented in Table 1 with GOES-9 and Table 2 with MTSAT-1R. The results of fog detection are verified based on surface observations collected at the 27 stations (see Fig. 1).

2) The DCD method

Fogs formed in nighttime over the Yellow Sea during the period from April to July 2004 were examined for obtaining the threshold values of the DCD. Table 1 shows the cases and their criteria of threshold for steam fog and advection fog by the DCD from GOES-9. The criteria are shown in the range of -3.8 to -2.0 K and total hourly mean is -2.8 K. In addition, it is shown in Table 2 that the hourly mean of DCD from MTSAT-1R has the range of -3.0 to -2.5 K and total hourly mean is -2.8 K. We used the date after April 2006 according to MTSAT-1R IR4 channel calibration report (Uesawa, 2006).

Ellrod (1995) had obtained the low and upper threshold values of DCD, which are -4 to -2 K, to detect coastal fog along the Gulf of Mexico, and the values by Lee *et al.* (1997) to detect fog over land are -3.5 to -1.0 K. In this study, we attempted to design the DCD method for the first step of detection. To decide the area that fog can occur, we took the

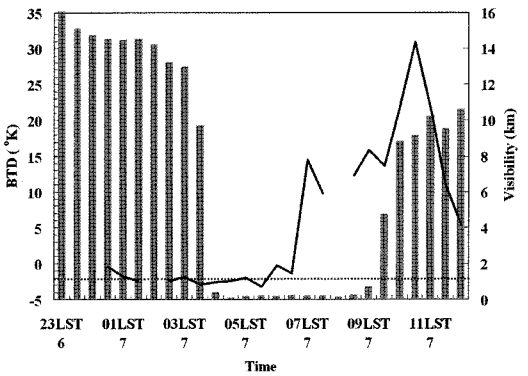

Fig. 4. Visibility(bar) derived from IORS observation data and a GOES-9 DCD(solid line) at Ieodo during the period from 23 LST 6 to 12 LST 7 April 2004. Dashed line represents DCD of -2.0 K.

threshold of -2.0 K. The steam fog case occurred at 03 LST 7 April 2004 [Fig 3 (a)] was applied to the DCD method. Fig. 4 shows the time evolution for visibility and DCD at the IORS. During a low visibility of less than 1 km, the DCDs were below -2.0 K from 02 LST until 09 LST. The SWIR increases the BT with sunrise from 07 LST. This indicates that this threshold of DCD should be used in the nighttime.

3) A radiation transfer model

To classify the fog and low stratus with the use of DCD method, we use the Rstar5b radiation transfer model developed by Nakajima and Tanaka (1988). This code simulates the radiation fields in the atmosphere-earth-ocean system for the spectral range between 0.3μm and 200μm using LOWTRAN-7. It is assumed that a plane parallel atmosphere is divided into 50 homogeneous sublayers with underlying ground or ocean surface.

In the present study, the top heights of fog and stratus are set at 1 km and 2 km respectively, and the cloud base for stratus is laid at 1 km, whereas that of fog is descended to the ground. The radiation transfer model is applied for different optical thickness and effective particle radius (EPR) as a method of Yum *et al.* (2004) and Yoo *et al.* (2005). The GOES-9 satellite zenith angle is set at 50 degree over the Korean Peninsula. We consider only water particles and assume a modified gamma distribution of spherical water particles within 20 μm radius. The optical thicknesses are given as 2, 4, 8, and 16. As the atmospheric sounding for the radiation transfer model, radiosonde observation of Gosan (33.28°N, 126.17°E) was used. Fig. 5 shows the BTD simulated by the model as a function of optical thickness for 4, 8, and 16 μm EPR. It is found that the simulated BTD is less sensitive for 16 μm EPR. The BTDs at all optical thickness for 16 μm EPR are simulated as about -4.0 K for fog and about -2.5 K for low stratus, and that for 4 or 8 μm EPR are less simulated than 16 μm EPR. This result shows that a BTD below -4.0 K is related to the occurrence of fog. However, in the present study, the area below -4.0 K is very limited,

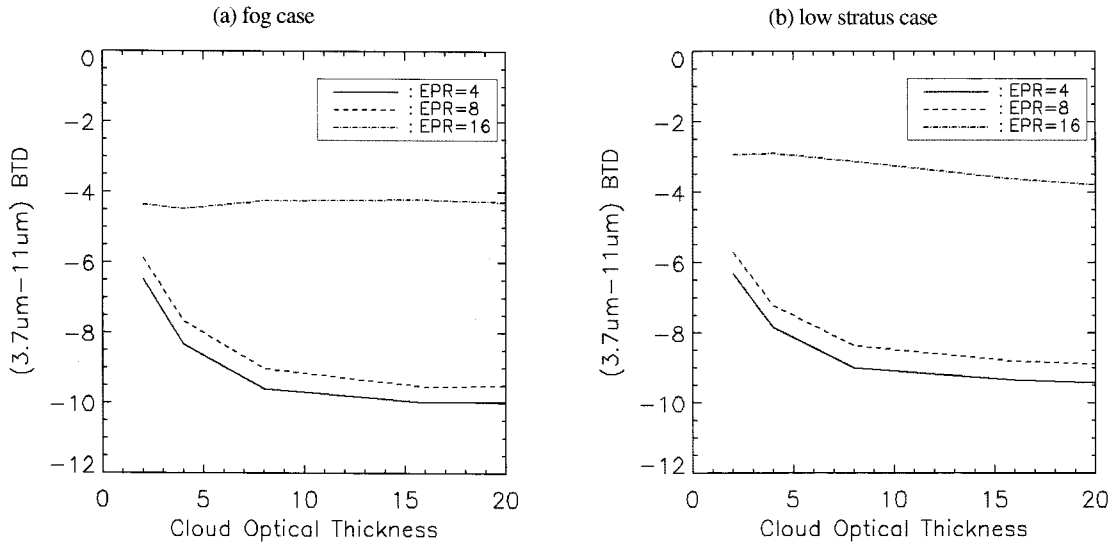

Fig. 5. The brightness temperature difference (BTD) between 3.9 μm and 10.7 μm simulated by radiation transfer model (rstar5b) as a function of optical thickness in each effective particle radius (EPR) for (a) fog case and (b) low stratus case. The solid line, dashed line, and dashed-dot line represent BTD for the 4, 8, and 16 of EPRs, respectively.

compared to the observation. In addition, there is not much in the BTDs for 4 and 8 μm EPR except for 16 μm EPR. Therefore, The BTD simulated by the radiation model has too many restrictions for use in separating fog. In this study, the difference of simulated BTDs for fog and low stratus was only considered as a reference, that the BTD for fog is bigger than that of low stratus. We attempted to use the wind speed by the QuikSCAT and texture from the horizontal distribution of brightness temperature to detect the broad area fog, which are hinted from the synoptic analysis of advection and steam fog over the Yellow Sea.

4. The combination of DCD with the use of QuikSCAT and the laplacian method

1) The classification of fog and low cloud with the use of QuikSCAT

As shown in Fig. 3, both the wind direction and wind speed are important for the formation of sea fog. To separate fog area from the results of DCD, Fig. 6 shows the area below the threshold value for DCD at 0530 LST and the wind vector in QuikSCAT at 0600 LST. There are dominant northerly winds over the Yellow Sea and, and a cold air burst can be expected in this situation. It can be seen that the foggy area with DCD is consistent with weak wind conditions. For the coastal fog, Heo and Ha (2004) reported the proper wind conditions for fog formation, which are less than 8 m s^{-1} in the southwestern part of the Yellow Sea, through a synoptic analysis. From the analysis of IORS data, it was found that the sea fog in the Yellow Sea was not dissipated in the wind condition less than 8 m s^{-1} (Fig. 3). This wind speed criteria is applicable to the separation of fog from low cloud.

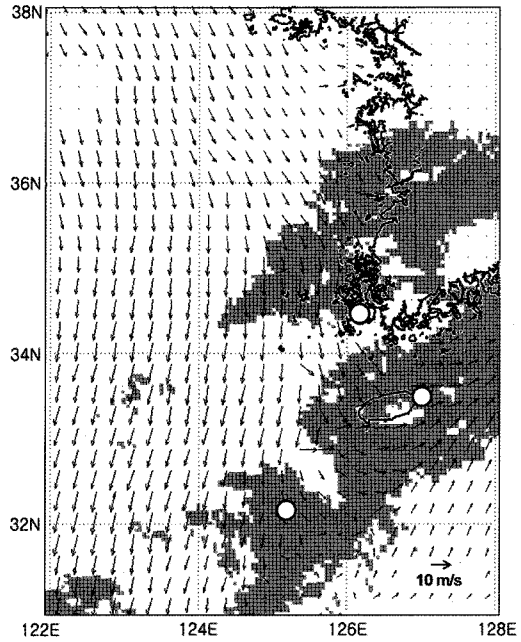

Fig. 6. QuikSCAT sea surface wind (vector) at 0600 LST and a GOES-9 DCD below -2.0 K (shaded area) at 0530 LST 7 April 2004. 'o' indicates fog observation station.

2) The homogeneity and laplacian

The top surface of fog area has a homogeneous aspect, compared to cloud (Bader *et al.*, 1995). Therefore, a laplacian method can be used to differentiate between low clouds and sea fog under the fog conditions determined by the DCD method. To compare the texture for homogeneity between the fog and the low cloud, we tried to analyze the frequency distribution of BTs for the cases of fog and low cloud. Fig. 7 shows the distribution of BTs at LWIR and SWIR from GOES-9 satellite during foggy day (10 June 2004) and stratus day (7 June 2004). Fog or stratus area was determined from where the value of the DCD is below -2.0 K. In the fog case, the distributions of BT for LWIR (a) and SWIR (c), which are narrow peak distribution, are concentrated at 286 K and 283 K, respectively (Fig. 7a and c). In the stratus case, however, the frequency distribution is widespread for the broad band (Fig. 7b

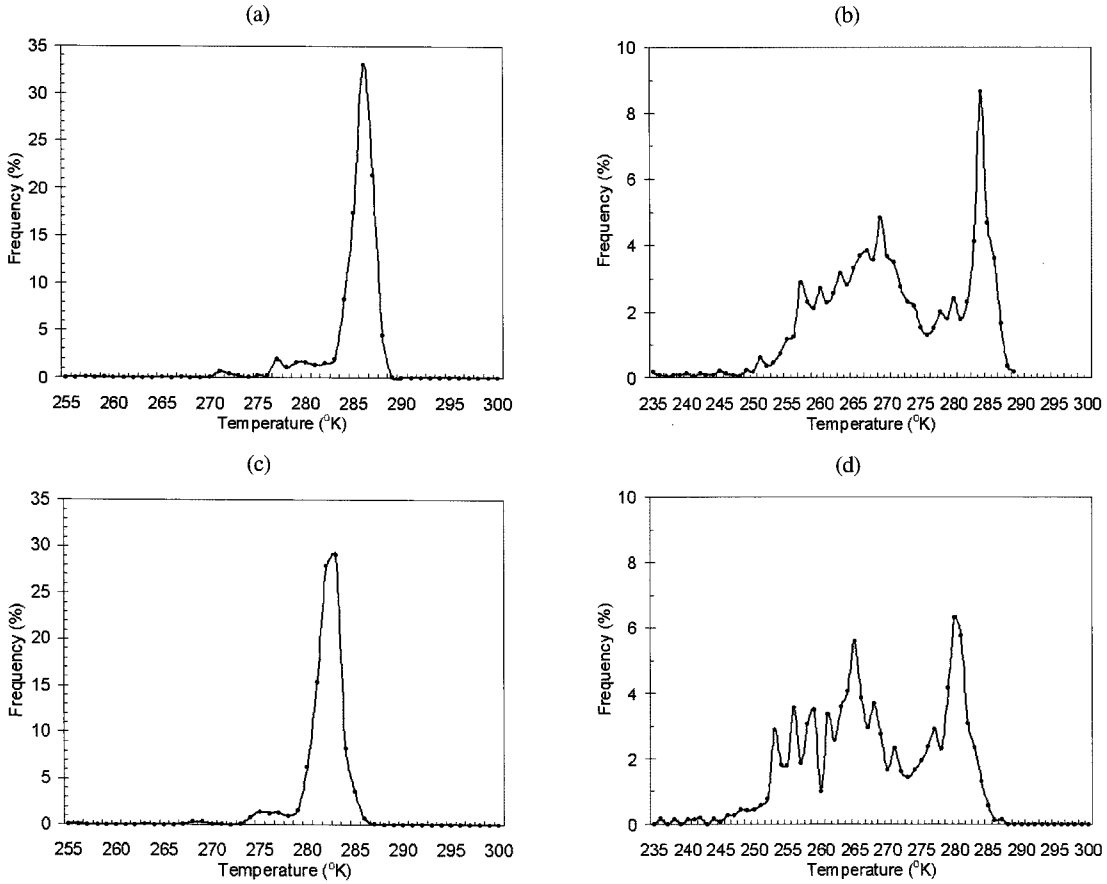

Fig. 7. The distributions of brightness temperature at 10.7 μm from GOES-9 satellite during (a) foggy day (2000 UTC 9 June 2004) and (b) stratus day (2000 UTC 6 June 2004). (c), (d) Same as (a) and (b), respectively, except for 3.9 μm.

and d). This result suggests that the fog is homogeneous rather than low cloud. In this study, we attempt to use the homogeneity measurement to distinguish the fog.

A laplacian method was used as a homogeneity distribution to separate low cloud from an area of fog and low cloud. In the laplacian of BT for LWIR and SWIR, laplacian smaller than the threshold indicates the foggy area, which is mainly due to homogeneous distribution for fog rather than cloud. The threshold value for laplacian was found to be 0.1 through comparison of visibility less than 1 km with ground fog observations for the cases days referred in Table 1 and Table 2 from this study. The number of fog observation used in this study is 28. Fig. 8 shows the horizontal laplacian of BT of GOES-9 LWIR (a), SWIR (b), MTSAT-1R LWIR (c) and SWIR (d) over the negative DCD (less than -2.0). Symbols such as '*', '●', '◉' represent fog observation points, fog free stations, and missing data stations, respectively.

A laplacian method can be used to differentiate between low clouds and sea fog under the fog conditions determined by the DCD method. The threshold value of laplacian operator in this study, 0.1, is empirically determined to discriminate the two. However, the threshold values for the laplacian should be more precisely defined with time-space variations in additional cases.

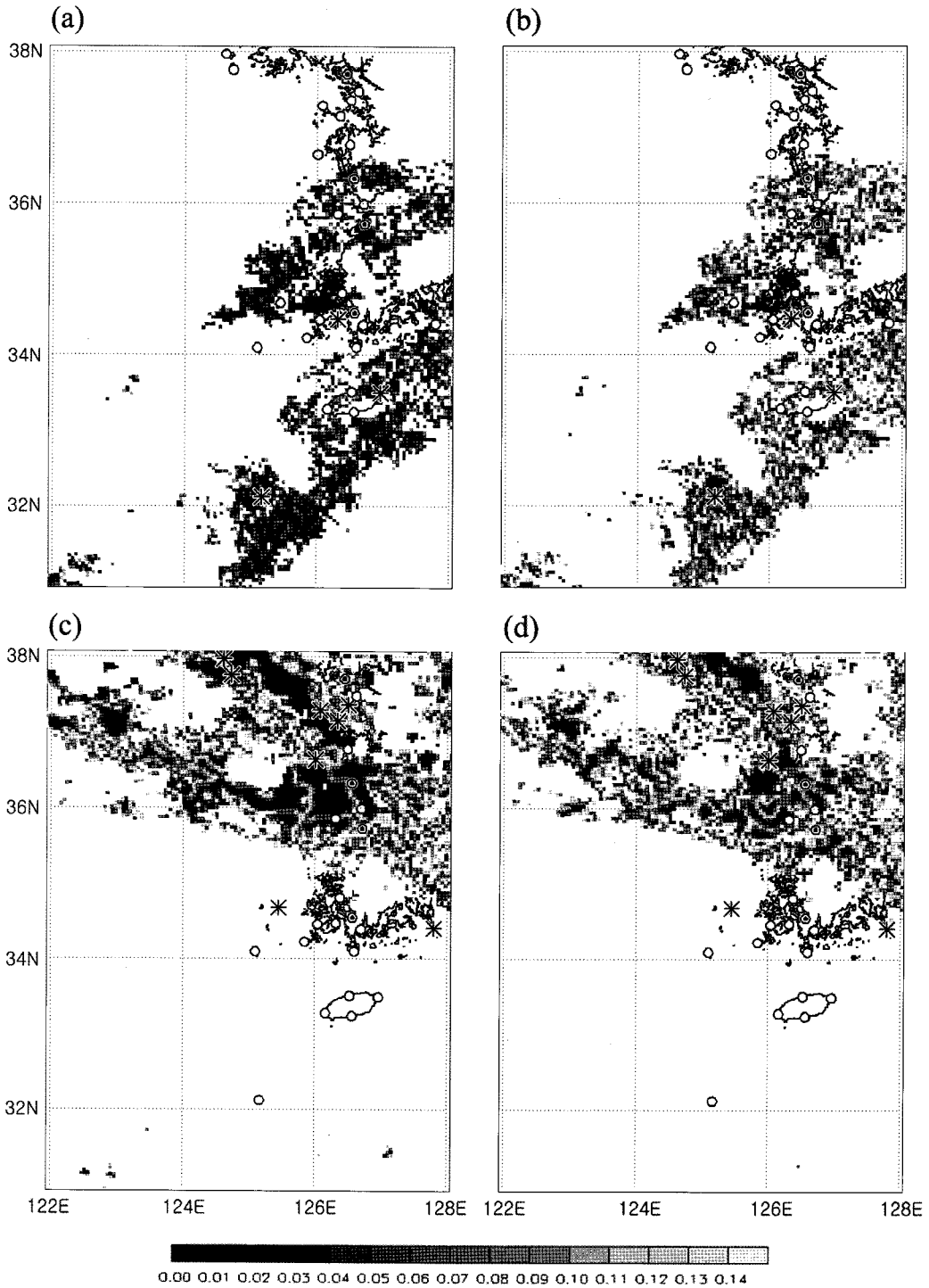

Fig. 8. Detection of fog and low cloud using the horizontal laplacian distribution of (a) BT_{CH4} and (b) BT_{CH2} at 2030 UTC 6 April 2004 from GOES-9 satellite. (c), (d) Same as (a) and (b), respectively, except for 2000 UTC 2 July 2006 from MTSAT-1R satellite. The symbols of '∗', '○' and '◉' represent the station where the visibility is less than 1 km (fog), larger than 1 km and not available, respectively.

5. The evaluation of the combined DCD method

1) The separation of foggy area with the check list method

In section 3 and 4, we described DCD, radiation model, the use of QuikSCAT wind speed, and texture. In the present study, to determinate the fog area, we made the check list table. The check lists for the detecting sea fog as shown in Table 3 consist of the DCD method, QuikSCAT wind speed and laplacian of BTLWIR. In evaluation, nine stations are used in the first step using the DCD method. In the second step, six stations are chosen within QuikSCAT wind speed of 8m s^{-1}. In the last step, six stations used for the calculation of the laplacian of BTLWIR. Through three steps, the three stations were obtained as fog stations. The stations selected by the check lists method are Ieodo, Sorido and Udo stations, represented bold within the Table 3. Table 4 is the same as Table 3 but the AWS wind speed is used in addition to QuikSCAT wind in the second

Table 3. The 3 steps of fog check lists of DCD, QuikSCAT wind speed and $\nabla^2(\mathbf{BT}_{CH4})$

Step	Validation point	Stations used for validation
1. GOES-9 DCD ($\leq$ -2.0 K)	9	Ieodo, Sorido, Udo, Gunsan, Maldo, Huksando, Mokpo, Gosan, Jeju
2. QuikSCAT wind speed ($\leq$ 8m s^{-1})	6	Ieodo, Sorido, Udo, Ongdo, Seonmido, Jeju
3. $\nabla^2(BT_{CH4})(\leq 0.1)$	6	Ieodo, Sorido, Udo, Budo, Jukdo, Mokpo

Table 4. The 3 steps of fog check lists of DCD, QuikSCAT + AWS wind speed and $\nabla^2(\mathbf{BT}_{CH4})$

Step	Validation point	Stations used for validation
1. GOES-9 DCD ($\leq$ -2.0 K)	9	Ieodo, Sorido, Udo, Gunsan, Maldo, Huksando, Mokpo, Gosan, Jeju
2. QuikSCAT & AWS wind speed ($\leq$ 8m s^{-1})	14	Ieodo, Sorido, Udo, Ongdo, Seonmido, Jeju, , Incheon, Palmido, Budo, Seosan, Gunsan, Gasado, Sohuksando, Wando
3. $\nabla^2(BT_{CH4})(\leq 0.1)$	6	Ieodo, Sorido, Udo, Budo, Jukdo, Mokpo

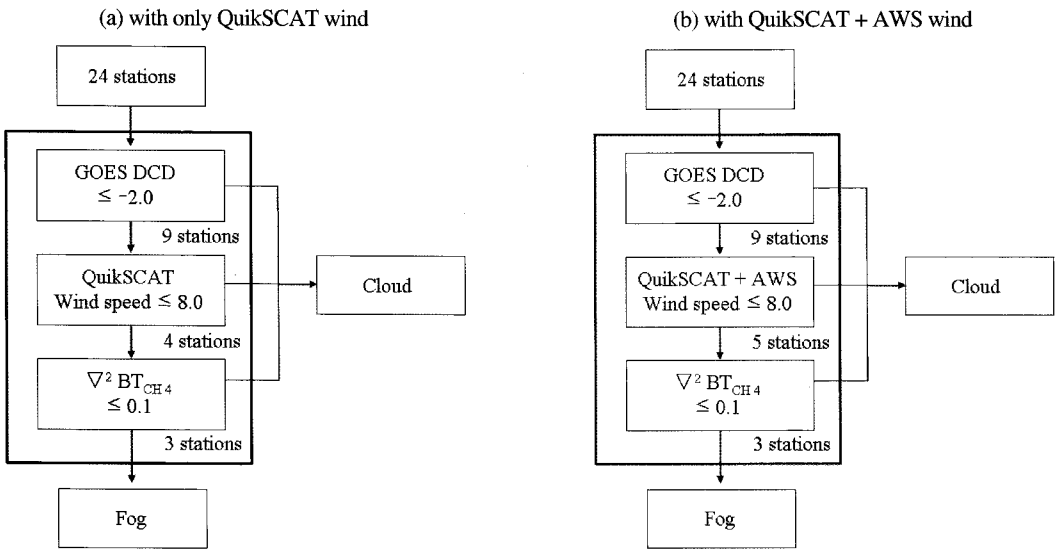

Fig. 9. Flow chart of check list method (a) with only QuikSCAT wind and (b) with QuikSCAT + AWS wind for steam fog case on 7 April 2004.

step. The number of stations was increased, but the same three stations were obtained again. Fig. 9 shows the flow chart of fog detection using the check lists method presented in Table 3 and Table 4.

2) The evaluation in the GOES-9 and MTSAT-1R satellite

In order to use the combined DCD method to the foggy area detection, we made a simple check list for the three steps as shown in Table 3. To measure the accuracy of the check list method in determining foggy area using GOES-9 images, we used, we used the validation statistics of skill scores. In the case of an event estimated fog occurrence (fog detected : Yes) and real fog occurrence (fog observed : Yes), then it is classified as hits (H); otherwise (fog observed : No) it is classified as misses (M). In the case of an event estimated fog nonoccurrence (fog detected : No) and real fog occurrence (fog observed : Yes), then it is classified as false alarm (F); otherwise (fog observed : Yes) it is classified as correct negative (C). The first type, exemplified by the Heidke skill score (HSS), tests the effectiveness in specifying the occurrence of fog. It can be written in the form:

$$HSS = (FC - EX)/(N - EX) \quad (2)$$

where $FC = (H + C)$,

$$EX = \frac{(H+F)(H+M)+(C+F)(C+M)}{N},$$

$$N = H + F + M + C$$

Range of HSS is $-2FM/(F^2 + M^2)$ to one, a perfect score = 1, no skill forecast = 0. Therefore, the HSS is 0.43 that means a 43% improvement in detection accuracy when compared to random chance (Table 5). The second type, probability of detection (POD) and probability of false detection (POFD), are fractions of observed events that were correctly predicted to exist and estimated events that are non-events, respectively:

$$POD = H/(H+M) \quad (3)$$

Table 5. Verification score formulates for GOES-9 satellite images

	Fog detected	
Fog observed	Yes	No
Yes	hits (**H**) : 42	misses (**M**) : 27
No	false alarms (**F**) : 39	correct negatives (C) : 218

a) HSS = 0.43, b) POD = 0.61, c) POFD = 0.15, d) TSS = 0.46, e) OR = 8.86

Range of POD is zero to one, a perfect score = 1.

$$POFD = F/(F+C) \quad (4)$$

Range of POFD is one to zero, a perfect score = 0. Slightly 61% of fogs that occurred were correctly detected to occur (POD = 0.61) and 15% of fog detections turned out to be false detection (no fog observed) (POFD = 0.15). The third type, true skill score (TSS) (Hanssen and Kuipers discriminant, Pierce's skill score) examines the ability of the check list to separate fog events from non-fog events and is defined as:

$$TSS = POD - POFD \quad (5)$$

Range of TSS is minus one to one, a perfect score = 1, no skill forecast = 0. The HSS is 0.46 that means the 46% of fog detections were able to separate the "yes" cases from the "no" cases (Table 5). Because the correct negative term dominates the others in the table, the TSS tends toward the POD when "yes" events are rare. The last type, odds ratio (OR) is greater than one when the hit rate (POD/1-POD) exceeds the false alarm rate (POFD/1-POFD):

$$OR = HC/FM = (POD/1-POD)/(POFD/1-POFD) \quad (6)$$

Range of OR is zero to infinity, a perfect score yields infinity, no skill system = 1, i.e. the ratio is greater than one when POD exceeds the False Alarm Rate. The odds of a "yes" detecting being correct are over 8.86 times greater than the odds of a "yes" detecting being incorrect in this result (Table 5).

To validate the check list method in determining foggy area using MTSAT-1R images, we used the

scoring method of the same as the validation method of GOES-9 images given in Table 6. The HSS is 0.46, which means a 46% improvement in detection accuracy when compared to random chance. In addition, Table 6 shows POD = 0.60, POFD = 0.14, TSS = 0.46 and OR = 9.21.

It induces a simultaneous increase (decrease) of POD and POFD for the threshold value of laplacian selected in a higher (lower) value than 0.1. Eventually, an accuracy of fog detection is decreased because an increase (decrease) of POFD (POD) is larger than that of POD (POFD). Therefore, the optimal threshold value of laplacian is chosen as 0.1 to discriminate fog from low cloud.

In order to compare DCD method with the combined DCD method, the skill scores of fog detection using only DCD method are presented in Table 7. It is evident in the HSS of both GOES-9 and MTSAT-1R satellites that the results of the present method increase a 5 ~ 6 % improvement in detection accuracy when compared to random chance rather than DCD. In addition, In the POFD, the present method has improved the discrimination of fog from low cloud. From the result of verifications, the present method is effective for fog detection and discrimination between fog and stratus.

In the bad performance case, we found that it can be noted that the check list method yields a poor performance over fog area when a low cloud case with coverage over 60% and ceiling heights between 300 m and 1200 m, or a 100% total cloud amount is observed.

Table 6. Same as in Table 1 except for MTSAT-1R

	Fog detected	
Fog observed	Yes	No
Yes	hits (H) : 60	misses (M) : 40
No	false alarms (F) : 39	correct negatives (C) : 244

a) HSS = 0.46, b) POD = 0.60, c) POFD = 0.14, d) TSS = 0.46, e) OR = 9.21

Table 7. Verification score for only DCD method

	GOES-9	MTSAT-1R
HSS	0.37	0.41
POD	0.68	0.68
POFD	0.25	0.23
TSS	0.43	0.45
OR	6.37	7.11

6. Summary and conclusion

Sea fog is frequently occurred in the Yellow Sea and the Korean coast during spring and summer season, which is responsible for marine accident and the problem of takeoff and landing. The monitoring by satellite data is strongly recommended for the detection of sea fog since numerical forecast skill and the MOS method have a limited utility for micro-scale and meso-scale structures of fog. In the present study, DCD method using the shortwave and longwave infrared channels of GOES-9 and MTSAT-1R satellites was applied to detect the foggy area. First, we used a radiation transfer model to investigate the possibility of fog detection with DCD method. By comparison of DCD between result of radiation model for the EPR=16 and satellite observation, it is found that the simulated DCD is not capable of separating fog from stratus due to very small detection area. In order to improve the detection method with the DCD, we designed combination method using the texture-related measurement and the weak wind condition as well as the DCD. The following threshold values are drawn from this study.

- We used the DCD method for the first step of detection. To decide the probable area of sea fog, we took the threshold of -2.0 K based on twelve cases over the Yellow Sea. This threshold value was used as a criteria to

determine fog and low cloud.

- The wind data of QuikSCAT were examined as weak wind conditions less than threshold of 8 m s^{-1} under stable condition of the surface wind around a fog event. This wind speed criteria is applicable to the separation of fog from low cloud.
- A laplacian calculation in the horizontal distribution of brightness temperature is proposed as a measure of homogeneity for the sea fog which is homogeneous rather than low cloud. The threshold values of laplacian of BT are obtained as 0.1 from sea fog cases over the Yellow Sea.

To validate the new combined DCD method in determining fog area, we applied the scoring methods such as Heidke skill score, probability of detection, probability of false detection, true skill score and odds ratio. The validation results reveal that the present method improves the sea fog detection and quantitatively separating fog from low cloud, which is seen in the scores of POFD. However, for the fog case with the high densed low cloud, the present method does not act to improve the separation of fog.

Acknowledgement

This work was supported by NASA and the Korea Meteorological Administration R&D program (CATER 2006-4103). This work was also supported by the Brain Korea 21 Project in 2007. We are grateful for providing Marine Meteorological Data in Ieodo Ocean Research Station by the Korean Ocean Research Development Institute.

References

Anthis, A. L. and A. P. Cracknell, 1999. Use of satellite images for fog detection (AVHRR) and forecast of fog dissipation (METEOSAT) over lowland Thessalia, Hellas. *Int. J. Remote Sensing*, 20: 1107-1124.

Bader, M. J., J. R. Forbes, J. R. Grant, R. B. Lilley, and A. J. Waters, 1995. *Images in weather forecasting: practical guide for interpreting satellite and radar data*. University Press, Cambridge.

Bendix, J., B. Thies, J. Cermak, and T. Nauss, 2005. Fog detection from space based on MODIS daytime data - A feasibility study. *Wea. Forecasting*, 20: 989-1005.

Byers, H. R., 1959. *General Meteorology*, 3rd Edition, McGraw Hill Book Co., Inc, 540pp.

Cermak, J. and J. Bendix, 2005. Fog / low stratus detection and discrimination using satellite data. *Proceeding of COST722 mid-term workshop on short-range forecasting methods of fog, visibility and low clouds*, 20 October 2005, Langen, Germany.

Cho, Y. K., M. O. Kim, and B. C. Kim, 2000. Sea fog around the Korean Peninsula. *J. Appl. Meteor.*, 39: 2473-2479.

Coakley, J. A. and F. P. Bretherton, 1982. Cloud cover from high-resolution scanner data: detecting and allowing for partially filled fields of view. *J. Geophys. Res.*, 87: 4917-4932.

Croft, P. J., R. L. Pfost, J. M. Medlin, and G. A. Johnson, 1997. Fog forecasting for the southern region: A conceptual model approach. *Wea. Forecasting*, 12: 545-566.

Ellrod, G. P., 1995. Advances in the detection and analysis of fog at night using GOES multispectral infrared imagery. *Wea.*

Forecasting, 10: 606-619.

Ellrod, G. P., 2000. Proposed improvements to the GOES nighttime fog product to provide ceiling and visibility information. *Preprints, 10th conf. on satellite meteorology and oceanography*, Long Beach, CA, Amer. Meteor. Soc., 454-456.

Eyre, J. R., J. L. Brownscombe, and R. J. Allam, 1984. Detection of fog at night using Advanced Very High Resolution Radiometer (AVHRR) imagery. *Meteorol. Mag.*, 113: 265-271.

Fu, G., J. Guo, S.-P. Xie, Y. Duan, and M. Zhang, 2006. Analysis and high-resolution modeling of a dense sea fog event over the Yellow Sea. *Atmos. Res.*, 81: 293-303.

Guidard, V. and D. Tzanos, 2005. Discrimination between fog and low clouds using a combination of satellite data and ground observations. *Proceeding of COST722 mid-term workshop on short-range forecasting methods of fog, visibility and low clouds*, 20 October 2005, Langen, Germany.

Heo, K. Y. and K. J. Ha, 2004. Classification of synoptic pattern associated with coastal fog around the Korean Peninsula. *J. Korean Metor. Soc.*, 40: 541-556 (in Korean with English abstract).

Hilliker, J. L. and J. M. Fritsch, 1999. An observations-based statistical system for warm-season hourly probabilistic forecasts of low ceiling at the San Francisco International Airport. *J. Appl. Meteor.*, 38: 1692-1705.

Hunt, G. E., 1973. Radiative properties of terrestrial clouds at visible and infra-red thermal window wavelengths. *Quarterly Journal of Royal Meteorological Society*, 99: 346-369.

Klein, S. A. and D. L. Hartmann, 1993. The seasonal cycle of low stratiform cloud. *J. Climate*, 6: 1587-1606.

Lee, T. F., F. J. Turk and K. Richardson, 1997. Stratus and fog products using GOES-8-9 3.9μm Data. *Wea. Forecasting*, 12: 606-619.

Liu, W. T., W. Tang, and R. Polito, 1998. NASA scatterometer provides global ocean-surface wind fields with more structures than numerical weather prediction. *Geophys. Res. Lett.*, 25: 761-764.

Liu, W. T., H. Hu, and S. Yueh, 2000. Interplay between wind and rain observed in hurricane Floyd. Eos, Trans. *Amer. Geophys. Union*, 81: 253-257.

Liu, W. T., H. Hu, Y. T. Song, and W. Tang, 2001. Improvement of scatterometer wind vectors-impact on hurricane and coastal studies, *in Proc. of WCRP/SCOR Workshop on Intercomparison and Validation of Ocean-Atmosphere flux Fields*, World Climate Research Programme, Geneva, 197-200.

Meteorological Satellite Center, 2002. *Analysis and use of meteorological satellite images.* Meteorological Satellite Center, 1st Edition, 195pp.

Nakajima, T. and M. Tanaka, 1988. Algorithms for radiative intensity calculations in moderately thick atmospheres using a truncation approximation, *J. Quant. Spectrosc. Radiat. Transfer*, 40: 51-69.

Park, H. S., Y. H. Kim, A. S. Suh, and H. H. Lee, 1997. Detection of fog and the low stratus cloud at night using derived dual channel difference of NOAA/AVHRR data. *Proceeding of the 18th Asian conference on remote sensing*, 20-24 Oct. Kuala lumpur, Malaysia.

Roach, W. T., 1994. Back to basics: Fog: Part 1 - Definitions and basic physics. *Weather*, 49: 411-415.

Sakaida, F. and H. Kawamura, 1996. HIGHERS-The

AVHRR-based higher spatial resolution sea surface temperature data set intended for studying the ocean south of Japan. *J. Oceanogr.*, 52: 441-455.

Scorer, R. S., 1986. *Cloud investigation by satellite.* Ellis Horwood Ltd., 314 pp.

Uesawa, D., 2006. Status of Japanese Meteorological Satellites and Recent Activities of MSC, *Proceedings of the 2006 EUMETSAT Meteorological Satellite Conference*, Helsinki, Finland, June 12-16, 2006.

Wentz, F. J., D. K. Smith, C. A. Mears, and C. L. Gentemann, 2001. Advanced algorithms For QuikSCAT and SeaWinds/AMSR. *Proceedings of IEEE 2001 International Geoscience and Remote Sensing Symposium*, 9-13 July 2001, Sydney, Australia.

Yoo, J. M., M. J. Jeong, and M. Y. Yun, 2005. Optical Characteristics of Fog in Satellite Observation (MODIS) and Numerical Simulation; Effect of Upper Clouds in Nighttime Fog Detection. *J. Korean Metor. Soc.*, 41: 639-650 (in Korean with English abstract).

Yum, S. S., S. N. Oh, J. Y. Kim, C. K. Kim, and J. C. Nam, 2004. Measurements of Cloud Droplet Size Spectra Using a Forward Scattering Spectrometer Probe (FSSP) in the Korean Peninsula. *J. Korean Metor. Soc.*, 40: 623-631 (in Korean with English abstract).